Quantum Electronics **51** (1) 84–94 (2021)

https://doi.org/10.1070/QEL17441

Measurements of quantum dot level populations using an optical waveguide

A.V. Tsukanov

Abstract. **A scheme is proposed for measuring electron level populations in a semiconductor quantum dot embedded in a multimode waveguide. The photon transmittance of the waveguide under steady-state pumping is shown to depend on the presence of an electron in the ground state of the quantum dot. The influence of waveguide, quantum dot, and photon source parameters on the electron detection process is examined. It is shown that, even at a moderate mode Q-factor (10^4 to 10^5), the measurement contrast and signal-to-noise ratio are rather high (above 10^4). The feasibility of using the proposed method for probing the state of a charge qubit is discussed.**

Keywords: *laser, waveguide, photons, quantum dot, measurement, transmittance, charge cubit.*

1. Introduction

Most measurement techniques used in experimental quantum physics are based on a spectroscopic approach, which offers the possibility of determining the energy of steady-state levels in a system under study and finding their broadening and population [1]. A steady-state response of a system (average number of transmitted or reflected photons as a function of external field frequency) carries information about its quantum state. First proposed in atomic optics, this approach was successfully adapted to solid-state quantum optics, which addresses issues pertaining to the interaction of microwave and optical photons with superconducting and semiconducting nanostructures, referred to as 'artificial atoms' [2, 3]. Semiconductor waveguides [4], microcavities [5], and quantum dots [6] can be integrated into photonic networks, which implement the concept of quantum internet proposed by Kimble in 2008 [7].

One-dimensional photonic crystals (1D PCs) have been widely used as compact, high-performance optical waveguide sensors for measuring the temperature, pressure, chemical composition, and concentration of a particular component of an analyte for more than a decade now. Their operating principle relies on the fact that photon transmittance depends on the volume of 1D PCs or the refractive index of the ambient medium [8]. Adsorption of molecules on the surface of a 1D PC increases its volume, shifting the frequencies of its eigenmodes. Scanning the frequency of a photon source allows one to calculate the shift and, hence, to identify the unknown substance. On the other hand, an object being tested can be located inside a 1D PC, and the purpose of investigation is then to determine its inner structure. Such objects include quantum dots (QDs) with a transition frequency near the photon frequency of a waveguide mode [9–11]. It is known that QDs can have electronic transitions with a frequency equal to the energy spacing between size quantisation levels in their conduction band (from a few to tens of millielectronvolts), excitonic transitions with a frequency corresponding to their band gap (about 1 eV), and combined (trionic) transitions. From the viewpoint of QD–1D PC interaction efficiency, the two types of transitions are equivalent, differing mainly in frequency range. In both cases, the mechanism of interaction is based on the conversion of an energy quantum from local QD excitation to a 1D PC mode photon and back again. Until recently, most researchers focused on investigation of excitonic transitions because their wavelength approaches the so-called telecom wavelength (1550 nm), a reference in waveguide optics. Besides, this range corresponds to frequencies of wavelength-tunable lasers, widely used in experiments. At the same time, an electron (or charge) qubit with electrical [12–14] and/or optical [15–24] control offers a number of advantages over an exciton qubit [25, 26], such as information storage reliability and the possibility of electrical control. The advent of submillimeter radiation sources (quantum cascade lasers based on heterostructures), including those under development by Alferov's team [27, 28], opened up the possibility of making analogous photonic systems with frequencies corresponding to electronic transition frequencies in a double QD (DQD). They can serve for both performing quantum operations on a charge qubit and measuring its state.

Our work demonstrates that an optical 1D PC waveguide supplemented with a low-intensity photon source (laser) offers the possibility of reliably measuring the electronic state of a QD being used as a charge qubit. Using standard Lindblad approach, we numerically simulate electron--photon dynamics in a multimode waveguide interacting with a QD. In an approximate Schrödinger approach, we derive an analytical expression for steady-state photon transmittance of a single-mode 1D PC with a QD. We calculate the measurement contrast and signal-to-noise ratio as functions of system parameters. Resonance measurements are shown to be more reliable than measurements in dispersion mode. An increase in waveguide mode density leads to an increase in contrast. Reliability of the method is shown to be determined by the laser pump energy, the energy of interaction of the QD with waveguide modes, and the photonic mode decay rate. Numerical simulation suggests the possibility of using lower Q

A.V. Tsukanov Valiev Institute of Physics and Technology, Russian Academy of Sciences, Nakhimovskii pr. 34, 117218 Moscow, Russia; e-mail: a-v-ts@mail.ru

Received 9 September 2020; revision received 19 October 2020
Kvantovaya Elektronika **51** (1) 84–94 (2021)
Translated by O.M. Tsarev

optical structures for qubit measurements than for coherent qubit control. In addition, we present results of assessing the effect of multiphoton components on measurement accuracy, which confirm the importance of maintaining mode population at a single-quantum level.

2. Model of a waveguide interacting with a charge qubit on a DQD

Quantum dots – semiconductor nanocrystals incorporated into a matrix [29], or regions with a positive effective potential produced by a combination of external electrostatic fields [30] – are known to allow individual electrons to be localised in a volume of space with a characteristic size of the order of their de Broglie wavelength. In such a case, an electron has discrete energy levels, which can be used as logical states of a qubit. To perform quantum operations on such a qubit, one should be able to distribute electron density between its logical states. To this end, one can use waveguide quantum fields controlling electron dynamics in the QD [24, 31]. In addition, entangled electron--photon states in QDs and 1D PCs (polaritons) are used to ensure communications within a network. For a system formed by a QD interacting with a 1D PC to be a unit cell of a quantum network (so-called quantum node), it is necessary to design a process for effectively measuring the electronic state of the QD.

Consider first an electron–photon structure consisting of a waveguide with a DQD incorporated into it (Fig. 1). A 1D semiconductor PC waveguide supports a set of photonic modes with frequencies ω_k ($k = 1...N$). A charge qubit based on the DQD, consisting of two QDs, A and B, contains one electron. The single QDs A and B coherently exchange an energy quantum with the kth mode. We assume that the QD A (B) has two one-electron states (ground state $|g_{\mathrm{A(B)}}\rangle$ and excited state $|e_{\mathrm{A(B)}}\rangle$, with energies $\varepsilon_{g\,\mathrm{A(B)}}$ and $\varepsilon_{e\,\mathrm{A(B)}}$), between which optical transitions are possible, with a frequency $\omega_{\mathrm{A(B)}} = \varepsilon_{e\,\mathrm{A(B)}} - \varepsilon_{g\,\mathrm{A(B)}}$. It is convenient to introduce designations for the energy differences between the ground and excited states of the QDs: $\Delta_g = \varepsilon_{g\,\mathrm{B}} - \varepsilon_{g\,\mathrm{A}}$ and $\Delta_e = \varepsilon_{e\,\mathrm{B}} - \varepsilon_{e\,\mathrm{A}}$. The frequency difference between the QDs is then $\omega_{\mathrm{B}} - \omega_{\mathrm{A}} = \Delta_e - \Delta_g$. The excited states of the QDs, lying near the edge of the potential barrier with a $U(\boldsymbol{r})$ profile, are hybridised as a result of electron tunnelling, whereas their ground states, located near the QD bottom, are isolated from each other. A weak laser field of frequency ω_{las} interacts with each waveguide mode, whose electric fields, $\boldsymbol{E}_k(\boldsymbol{r})$, have antinodes in the DQD region.

To date, several approaches to the synthesis and control of various types of semiconductor DQDs have been demonstrated. Most research effort has focused on a semiconductor implementation of crystalline DQDs in an In(Al)GaAs solid solution on GaAs. Besides, DQDs based on silicon–germanium structures are under investigation. Depending on the orientation of the axis between the centres of the QDs relative to the surface of the structure, there are lateral and vertical DQDs. Lateral DQDs, whose axis is parallel to the substrate surface, are grown in seed pits made on the substrate [32, 33]. To synthesise vertical DQDs, whose axis is perpendicular to the substrate surface, use is made of QD growth in a second layer just above the QD in the first layer, with its shape and dimensions reproduced [29, 34–36]. It is worth noting that the formalism and results obtained in this study correspond to a wider class of quantum-optical structures with qubits, which can be thought to include not only single-electron and single-exciton semiconductor QDs but other solid-state nanosystems (see a recent review by Chatterjee et al. [37]), in particular, (a) DQDs based on a singly ionised pair of phosphorus donors in silicon, (b) DQDs based on a singly ionised pair of colour centres in diamond, and (c) natural molecular ions adsorbed on the surface of a waveguide.

In the fabrication of 1D PCs, DQD-containing gallium arsenide wafers are used as workpieces. Using electron beam lithography and chemical etching, a 1D PC body (rod) is cut

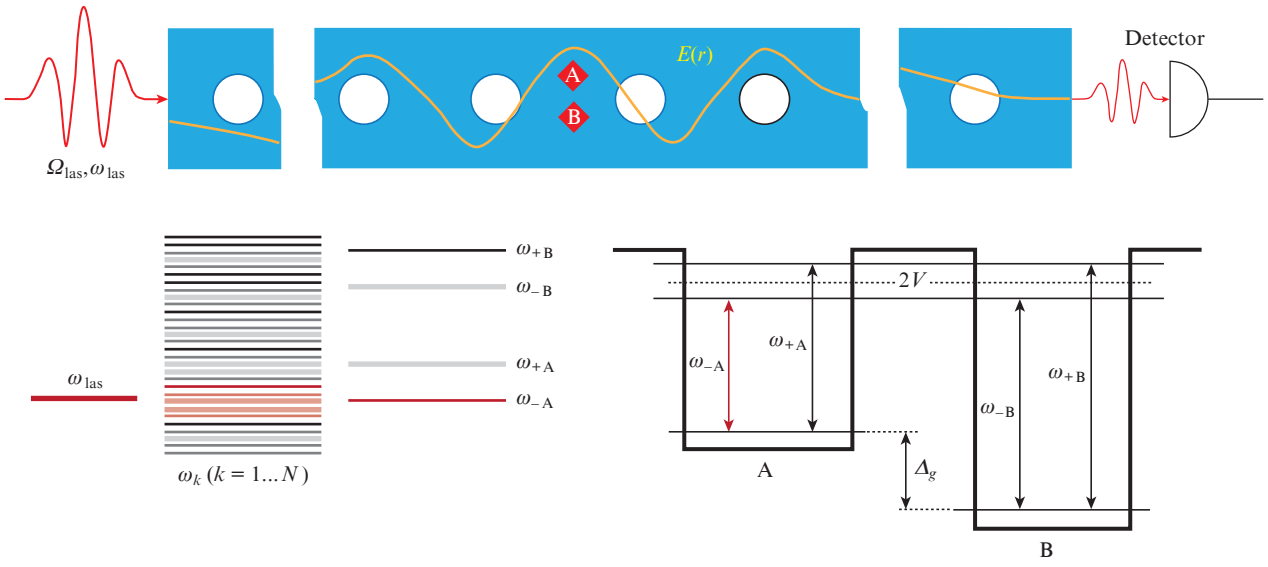

Figure 1. Schematic of a measuring device comprising a 1D photonic crystal with a single-electron DQD, photon source (laser), and photon detector. The DQD is produced in the region between holes of the 1D PC lattice in an antinode of the $E(r)$ amplitude of one or a few modes close in frequency to one of the transitions of the DQD ($\omega_{-\mathrm{A}}$ in this case) (upper panel). Schematic illustrating the relationship between the laser, 1D PC, and DQD frequencies in the case of resonance between the frequencies of the laser and the lower transition in the QD A and diagram of the DQD potential profile and energy levels in the case of exact resonance ($\Delta_e = 0$) between the excited states of the QDs A and B. The dashed lines show the position of the excited state levels of isolated QDs (lower panel).

from a wafer, and then ion etching is used to produce a 1D periodic lattice (chain) of holes in it, which ensures interference of electromagnetic waves inside the 1D PC and is responsible for the band character of its spectrum [8, 9]. Another type of 1D PC is a waveguide formed by an extended linear defect in a lattice of holes of a 2D photonic crystal (a sequence of missing holes or holes with a different diameter) [10, 11]. The two structures have a quasi-discrete spectrum of photonic modes and roughly the same quality factor. The position of the DQD in the wafer can be determined using marks on its surface [29], which allows the coordinates of the holes in the lattice to be chosen so that the DQD is located in an antinode of 1D PC modes with frequencies close to the transition frequency of one of the QDs. Other, less widespread, materials are SiGe, GaP, SiN, and C (diamond), but in this case a DQD-containing (In)GaAs crystal can only be placed on the surface of the 1D PC, which will sharply reduce the electron–photon interaction energy.

In a frame of reference fixed to laser light, the electron–photon Hamiltonian has the form

$$\begin{aligned} H = & \sum_{k=1}^{N} \delta_k a_k^{\dagger} a_k + \Delta_g |g_{\mathrm{B}}\rangle\langle g_{\mathrm{B}}| + \delta_{\mathrm{A}} |e_{\mathrm{A}}\rangle\langle e_{\mathrm{A}}| \\ & + (\Delta_g + \delta_{\mathrm{B}}) |e_{\mathrm{B}}\rangle\langle e_{\mathrm{B}}| - V[|e_{\mathrm{A}}\rangle\langle e_{\mathrm{B}}| + |e_{\mathrm{B}}\rangle\langle e_{\mathrm{A}}|] \\ & - \sum_{k=1}^{N} [\Omega_{\mathrm{A}k} |e_{\mathrm{A}}\rangle\langle g_{\mathrm{A}}| a_k + \Omega_{\mathrm{B}k} |e_{\mathrm{B}}\rangle\langle g_{\mathrm{B}}| a_k + \mathrm{h.c.}] \\ & + \sum_{k=1}^{N} \Omega_{\mathrm{las}k} (a_k^{\dagger} + a_k), \end{aligned} \tag{1}$$

where a_k is the annihilation operator for a photon in the kth mode; $\delta_k = \omega_k - \omega_{\mathrm{las}}$, $\delta_{\mathrm{A}} = \omega_{\mathrm{A}} - \omega_{\mathrm{las}}$, and $\delta_{\mathrm{B}} = \omega_{\mathrm{B}} - \omega_{\mathrm{las}}$ are the detunings of the kth mode, QD A, and QD B from the laser frequency; $V \sim \langle e_{\mathrm{A}} | U(\boldsymbol{r}) - \varepsilon_{e\mathrm{A}} | e_{\mathrm{B}} \rangle$ is the energy (rate) of single-electron tunnelling between the excited states of the QDs [38]; $\Omega_{\mathrm{A(B)}k} = \langle e_{\mathrm{A(B)}} | -e\boldsymbol{E}_k(\boldsymbol{r})\boldsymbol{r} | g_{\mathrm{A(B)}} \rangle$ is the energy (rate) of exchange of a quantum between the QD A (B) and the kth mode; and $\Omega_{\mathrm{las}k} \sim \int \boldsymbol{E}_{\mathrm{las}}(\boldsymbol{r})\boldsymbol{E}_k(\boldsymbol{r})\mathrm{d}\boldsymbol{r}$ is the energy (rate) of exchange of a quantum between a laser field of amplitude $\boldsymbol{E}_{\mathrm{las}}(\boldsymbol{r})$ and the kth mode. Let us introduce the rates of incoherent processes, such as relaxation and dephasing, as well. The rate of photon removal (relaxation) from the kth mode of a waveguide to a continuum is κ_k; the rate of a nonradiative decay of the excited electron state of the QD A (B), due to uncontrolled interaction with phonons, is $\gamma_{\mathrm{rA(B)}}$; and the rate of dephasing related to stochastic fluctuations of the transition frequencies in the QDs is $\gamma_{\mathrm{dA(B)}}$. All parameters of Hamiltonian (1) can be calculated in a microscopic model or found experimentally.

Methods for controlling the spectrum of both single and double QDs by applying a local electric field have been known for two decades now and are well developed. In addition to tuning transition frequencies of individual QDs, it is possible to vary the relative position of electron levels in neighbouring QDs. This allows one to gradually vary the overlap between the electron orbitals of the QDs, thereby stimulating or suppressing electron tunnelling between the QDs. For example, Stinaff et al. [25] illustrated this mechanism of controlling the internal state of an 'artificial molecule' in the form of a DQD of two tunnel-coupled crystalline InGaAs/GaAs QDs. Its emission spectrum as a function of external field strength demonstrates a set of avoided crossings indicative of the hybridisation of electron orbitals as their energies approach resonance (coincidence). This provides convincing evidence for the existence of DQDs with identical energies in fields with amplitudes from 40 to 60 kV cm^{-1}. These results were confirmed in other studies [32–36]. It is worth noting that, causing a natural shift of excited state levels of a DQD and suppressing tunnel coupling between the QDs in the absence of a field, structural asymmetry [36] ensures reliable storage of the state of the qubit [24] as long as it is not involved in the active stage of the quantum algorithm. In other words, the field that tunes the excited state levels of the left and right QDs to resonance should be applied only when implementing some gate with direct participation of the given qubit.

The dynamics of an electron–photon system can be described by the Lindblad equation, whose solution is the time dependence of its density matrix, $\rho(t)$, for a particular initial state $\rho(0)$:

$$\begin{aligned} \frac{\mathrm{d}\rho}{\mathrm{d}t} = & -\mathrm{i}[H,\rho] + \sum_{k=1}^{N} \kappa_k D(a_k) + \gamma_{\mathrm{rA}} D(|g_{\mathrm{A}}\rangle\langle e_{\mathrm{A}}|) \\ & + \gamma_{\mathrm{rB}} D(|g_{\mathrm{B}}\rangle\langle e_{\mathrm{B}}|) + \gamma_{\mathrm{dA}} D(|e_{\mathrm{A}}\rangle\langle e_{\mathrm{A}}| - |g_{\mathrm{A}}\rangle\langle g_{\mathrm{A}}|) \\ & + \gamma_{\mathrm{dB}} D(|e_{\mathrm{B}}\rangle\langle e_{\mathrm{B}}| - |g_{\mathrm{B}}\rangle\langle g_{\mathrm{B}}|). \end{aligned} \tag{2}$$

Dissipative photonic and electronic processes can be modelled by the Lindblad operators $D(O) = O\rho O^{\dagger} - [O^{\dagger}O,\rho]/2$. We take the following basis states:

$$|j\rangle = |m\rangle \otimes \prod_{k=1}^{N} |n_k\rangle,$$

where $m = g_{\mathrm{A}}, g_{\mathrm{B}}, e_{\mathrm{A}}$, and e_{B} are the states of the DQD and n_k is the number of photons in mode k. We are interested in the regime where the external field has a small amplitude and, hence, the probability of excitation of the system is low, and examine the average number of photons at the waveguide output (transmittance),

$$T = \left\langle \sum_{k=1}^{N} a_k^{\dagger} a_k \right\rangle, \tag{3}$$

as a function of parameters of the system, especially of the excitation laser frequency. Numerical analysis of the spectral features due to the localisation of the qubit electron in the ground state of the QD A or B allows one to investigate the influence of external and internal factors on the feasibility of measuring the state of the qubit.

The spectrum of the system can be calculated in a different way as well, by solving the Schrödinger equation

$$\mathrm{i}\frac{\partial |\Psi\rangle}{\partial t} = H_{\mathrm{eff}} |\Psi\rangle$$

with an effective Hamiltonian obtained from Eqn (1) by making the $\delta_k \to \delta_k - \mathrm{i}\kappa_k$, $\delta_{\mathrm{A}} \to \delta_{\mathrm{A}} - \mathrm{i}\gamma_{r\mathrm{A}}$, and $\delta_{\mathrm{B}} \to \delta_{\mathrm{B}} - \mathrm{i}\gamma_{r\mathrm{B}}$ substitutions and adding imaginary terms that describe relaxation processes. Assuming that the average number of photons in the waveguide modes is considerably less than unity, we restrict our consideration to a vacuum state ($n_k = 0$) and a single-photon state of each mode. The dimensionality of the

eigenvector space is $2N + 4$. The main component of the wave vector

$$|\Psi\rangle = \sum_{j=1}^{2N+4} c_j |j\rangle$$

is the state

$$|1\rangle = |g_A\rangle \otimes \prod_{k=1}^{N} |0_k\rangle \quad \text{or} \quad |2\rangle = |g_B\rangle \otimes \prod_{k=1}^{N} |0_k\rangle,$$

corresponding to the waveguide modes being in the vacuum state and the DQD being in one of the electron ground states. The state

$$|3\rangle = |e_A\rangle \otimes \prod_{k=1}^{N} |0_k\rangle \quad \text{or} \quad |4\rangle = |e_B\rangle \otimes \prod_{k=1}^{N} |0_k\rangle$$

is identified with electronic excitations of the DQD. The other $2N$ states describe single-photon excitation of a particular mode and the DQD in its ground state. Since a steady-state solution meets the constraint

$$\frac{\partial |\Psi\rangle}{\partial t} = 0 \quad \text{or} \quad \dot{c}_j = 0,$$

the initial differential equation reduces to a homogeneous algebraic system of equations for probability amplitudes. Taking $c_1 \approx 1$ or $c_2 \approx 1$, which corresponds to the presence of an electron in the QD A or B, we can reduce the order of this system by one, transforming it into an inhomogeneous algebraic system. Further calculation of probability amplitudes for single-photon components leads to finding the photon transmittance of the structure:

$$T = \sum_{j=5}^{2N+4} |c_j|^2.$$

Examining this function, we can determine characteristic frequencies of the electron–photon hybrid system, which depend on the state of the qubit.

Assume that a DQD with an electron in the ground state of the QD A actively interacts with only one mode. Then, in the weak field approximation indicated above, the spectroscopic signal has the following form (where the subscript specifying the mode is omitted):

$$T_A = \Omega_{las}^2 \left| \frac{(\delta_A - i\gamma_A)\Delta_B - V^2(\delta + \Delta_g - i\kappa)}{\Delta_A \Delta_B - V^2(\delta - i\kappa)(\delta + \Delta_g - i\kappa)} \right|^2,$$

$$\Delta_A = (\delta_A - i\gamma_A)(\delta - i\kappa) - \Omega_A^2, \qquad (4)$$

$$\Delta_B = (\delta_B + \Delta_g - i\gamma_B)(\delta + \Delta_g - i\kappa) - \Omega_B^2.$$

If there is no interaction between the QD A and the mode ($\Omega_A = 0$), the function $T_A(\omega_{las})$ has the form of a Lorentzian whose maximum is located at the frequency of the mode. If $\Omega_A \neq 0$ and tunnel coupling between the excited states of the QDs A and B is blocked ($V = 0$), relation (4) transforms into a well-known formula for the response function in the Jaynes–Cummings model. This model describes interaction between a two-level system (the QD A in our case) and a waveguide mode. If the frequency of the QD A is exactly identical to that of the mode, the two resonance frequencies at which the denominator in (4) has a minimum correspond to the frequencies of the first Jaynes–Cummings doublet. They differ from the frequency of the QD A by $\pm\,\Omega_A$ (vacuum Rabi splitting [39]). Thus, for laser radiation of frequency $\omega_{las} = \omega_A$ there is a so-called photon blockade effect: if one energy quantum enters the structure, other photons with this frequency will be reflected from the structure, which will lead to a sharp drop in transmitted signal intensity. This feature of the spectral response indicates the presence of an electron in a QD with a transition frequency corresponding to the laser frequency at which an intensity collapse is observed. This effect underlies the operating principle of a single-photon transistor, whose current capacity depends on the presence or absence of a photon in the mode. If $V \neq 0$ and $\Delta_e = 0$, but $\Omega_B = 0$, the mode interacts with two electronic transitions whose frequencies differ from that of the QD A by $\pm V$. Finally, at $\Omega_B \neq 0$ an electron can undergo an optical tunnelling transition to the QD B as well, and the spectral picture becomes even more complex. We assume that the QDs A and B differ in physical properties to the extent that the energy difference between their ground states meets the asymmetry condition $\Delta_g \gg \max[V, \Delta_e, \Omega_{A(B)}]$. The DQD then has two sets (doublets) of transition frequencies in each QD (Fig. 1):

$$\omega_{\pm A(B)} = \omega_{A(B)} \pm \sqrt{V^2 + \Delta_e^2/4}\,. \qquad (5)$$

Since the separation between the doublet frequencies $\omega_{\pm A}$ and $\omega_{\pm B}$ is rather large, scanning the laser frequency around one of the doublets and subsequent examination of the spectroscopic response of the 1D PC makes it possible to answer the question of whether an electron is present in the corresponding QD. Indeed, the presence or absence of photon blockade at $\omega_{las} \approx \omega_{\pm A}$ ($\omega_{las} \approx \omega_{\pm B}$) unambiguously points to the presence or absence of an electron in the QD A (B), which is equivalent to measuring the qubit. The next two sections deal with quantitative characteristics of the measurement process and their dependences on parameters of the DQD, 1D PC, and laser.

3. Calculation of 1D PC transmittance in the single-photon multimode regime

Like in a single-electron transistor, the current through which is controlled by interaction between tunnelling electrons and the charge qubit, the photon transmittance of a 1D PC depends on the spatial position of an electron in the qubit. At the same time, whereas the energy of Coulomb interaction between two electrons is only determined by the distance between their localisation regions (QD island in the transistor and one of the QDs of the DQD charge qubit), electron–photon interaction is determined by both the position of the qubit relative to the antinode of the mode and electronic transition frequencies in each QD. It is the latter circumstance which allows one to reliably determine the spatial position of an electron in an asymmetric DQD. Consider how the spectrum of a waveguide varies when the transition frequency in the QD A is close to the frequency of one of the waveguide modes. As found out above, with allowance for tunnel splitting in the DQD, each QD in it has two optical frequencies, which differ from its unperturbed frequency by $\pm\sqrt{V^2 + \Delta_e^2/4}$. For definiteness, hereafter we will consider the lower one (ω_{-A}) as a resonance frequency. Parameters of the DQD and waveguide

are given in units of the frequency ω_A (40–80 meV) and correspond to experimentally observed values.

Figure 2a shows photon transmittance as a function of photon frequency for a waveguide interacting with the QD A (T_A) and a waveguide noninteracting with the QD A (T_{wg}). In the latter case, the spectrum of the waveguide has the form of a set of equidistant peaks, with a free spectral range (FSR) set by the waveguide length. It was chosen so that the Lorentzians corresponding to modes were well discernible in the T_{wg} curve. According to the theory of the coherent Jaynes–Cummings effect, if the frequency ω_{-A} of the electronic transition in the QD A is near the frequency of a waveguide mode we should obtain a vacuum Rabi splitting of the mode into a doublet of polariton states. However, Fig. 2a shows a triplet consisting of such a doublet and a central line at a mode frequency of the waveguide with no QDs. This feature can be observed experimentally [9] and is due to incoherent processes in the QD A. This is evidenced by the dependence of the intensity of the central peak on the decay rate γ_r of the excited electronic state of the QD A, due to interaction with a phonon reservoir (in Section 3, we took $\gamma_r = \gamma_d = \gamma$).

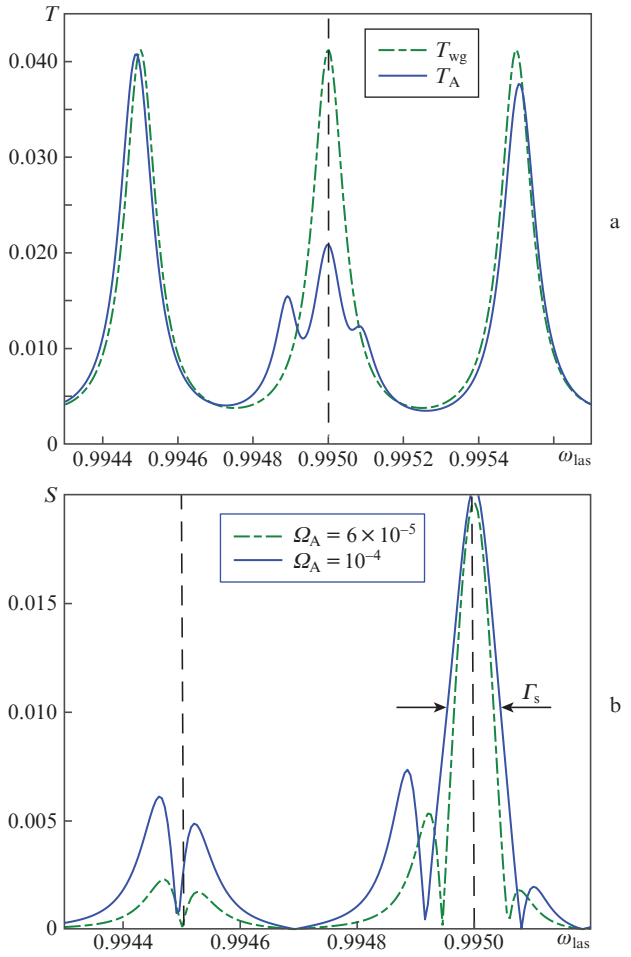

Figure 2. (a) Photon transmittance as a function of laser frequency for an empty waveguide and a waveguide interacting with an electronic transition in the QD A and (b) measurement contrast of the waveguide as a function of laser frequency at two energies of interaction between the modes and QD A at FSR = 5×10^{-4}, $\Omega_{las} = 10^{-5}$, $\Omega_A = 10^{-4}$, $\kappa = 5\times10^{-5}$, $\Delta_g = 10^{-3}$, $\Delta_e = 0$, $V = 5\times10^{-3}$, and $\gamma = 2\times10^{-5}$. Here and in the other figures, all parameters are given in units of the transition frequency in the QD A.

Here, it is comparable to the rates of coherent processes. Reducing γ_r by an order of magnitude causes the central peak to disappear (see Section 4). The asymmetry of the doublet peaks is caused by the slight frequency detuning between the mode and QD A. In addition, the frequencies of neighbouring modes undergo a dispersion shift $\sim \Omega_A^2/\mathrm{FSR}$. Following Kim et al. [40], to quantitatively characterise the effect of the QD A on the spectrum of the waveguide we introduce measurement contrast S as the difference between transmittances T_{wg} and T_A:

$$S = |T_A - T_{wg}|. \tag{6}$$

It can be seen that the function S has the highest value for the mode with a frequency $\omega_c = 0.995$, which resonantly interacts with the QD A. The frequency at which the maximum contrast S_{max} is observed coincides with the frequency of the unperturbed mode. Finding the contrast maximum, we can calculate the signal-to-noise ratio, SNR = S_{max}/Γ_S, which characterises the measurement quality factor. The width of the maximum, Γ_S, is roughly equal to that of the peak in T_A. At the same time, dispersion shifts of neighbouring modes also lead to noticeable changes in the level of the signal, which is 25% of the maximum value S_{max} for the mode in resonance with the QD A. For the next pair of waveguide modes, dispersion shifts do not exceed 10% of the maximum.

The magnitudes of transmittances are determined by the ratio of the pump rate Ω_{las} to the dissipation rate κ, which ensures that conditions for the subphoton regime are fulfilled for $\Omega_{las}/\kappa \leqslant 1$. As follows from the calculation results presented in Fig. 2b, the peak S_{max} and its width Γ_S are weak functions of interaction energy Ω_A, even though on the whole the S curve has a tendency to decrease, with a reduction throughout the frequency range studied. The function S_{max} approaches its asymptotic value even at relatively low Ω_A energies. The effect of FSR is far more noticeable: in Fig. 3, S_{max} rises markedly as neighbouring modes approach each other.

In this case, the single-mode Jaynes–Cummings model is no longer applicable because resonance interaction condi-

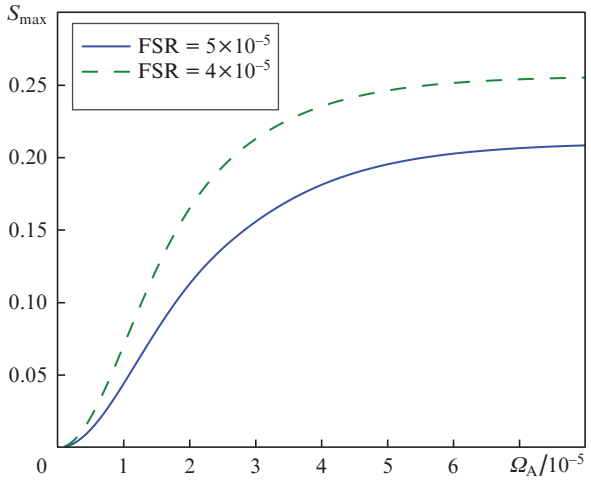

Figure 3. Maximum measurement contrast as a function of the energy of interaction between the mode and QD A at two free spectral range values, $\omega_{las} = 1 - V$, $\Omega_{las} = 10^{-5}$, $\kappa = 3\times10^{-5}$, $\Delta_e = 0$, $\Delta_g = 10^{-2}$, $V = 5\times10^{-3}$, and $\gamma = 2\times10^{-5}$.

tions are fulfilled for several waveguide modes with frequencies near the transition frequency in the QD A. An increase in photon mode density, accompanied by a decrease in free spectral range to FSR $\approx \kappa$, leads to a transformation of the discrete spectrum to a quasi-continuous one, consisting of a sequence of allowed and forbidden bands. Note that, for all frequencies in an allowed band, the level of the signal at the waveguide output is essentially the same. The spectral response takes a spiky shape, observed in real 1D waveguide structures [41]. The heights of the peaks corresponding to modes turn out to be insignificant relative to the average signal and decrease to zero as the modes further approach each other.

QD–waveguide interaction leads to the formation of a single minimum, whose depth and width depend on the parameter Ω_A: the stronger the QD–mode interaction, the larger and broader the minimum (Fig. 4). Besides, there is strong dispersion interaction with the rest of the spectrum of the waveguide: the peaks shift upwards and their envelope becomes curved. Clearly, the maximum contrast corresponds to the frequency at which the function T_A has the minimum. It can shift in response to changes in the structure of the excited state doublet of the DQD, due to variations in the tunnelling energy and the difference in excited state energy, Δ_e, between the QDs A and B.

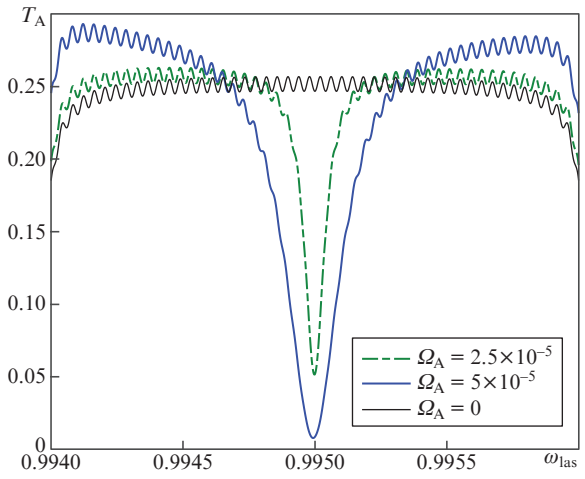

Figure 4. Photon transmittance as a function of laser frequency for a waveguide with a quasi-continuous spectrum at three energies of interaction with the QD A, FSR $= 4\times10^{-5}$, $\Omega_{las} = 10^{-5}$, $\kappa = 3\times10^{-5}$, $\Delta_e = 0$, $\Delta_g = 10^{-2}$, $V = 5\times10^{-3}$, and $\gamma = 2\times10^{-5}$.

Laser frequency scanning leads to expected results, presented in Fig. 5 and determined by the dependence of the electronic doublet energies, $\varepsilon_\pm = \varepsilon_{eA} + \Delta_e/2 \pm \sqrt{V^2 + \Delta_e^2/4}$, on these parameters. If the condition for resonance tunnelling of an excited electron between the QDs A and B ($\Delta_e = 0$) is exactly fulfilled and V increases from zero, the response demonstrates linear dependences of the two resonance frequencies of the QD A, which reflect the splitting of the doublet levels. If V is maintained constant and the difference Δ_e is varied around zero, with increasing positive (negative) deviation the lower (higher) frequency of the DQD approaches the electronic transition frequency in an isolated QD A. The other frequency, related to electron localisation in the QD B, deviates linearly from the symmetry point, and the peak gradually disappears. By analysing spectrograms obtained by varying the internal structure of the DQD with the use of an electric field, one can calculate parameters of Hamiltonian (1) via interpolation.

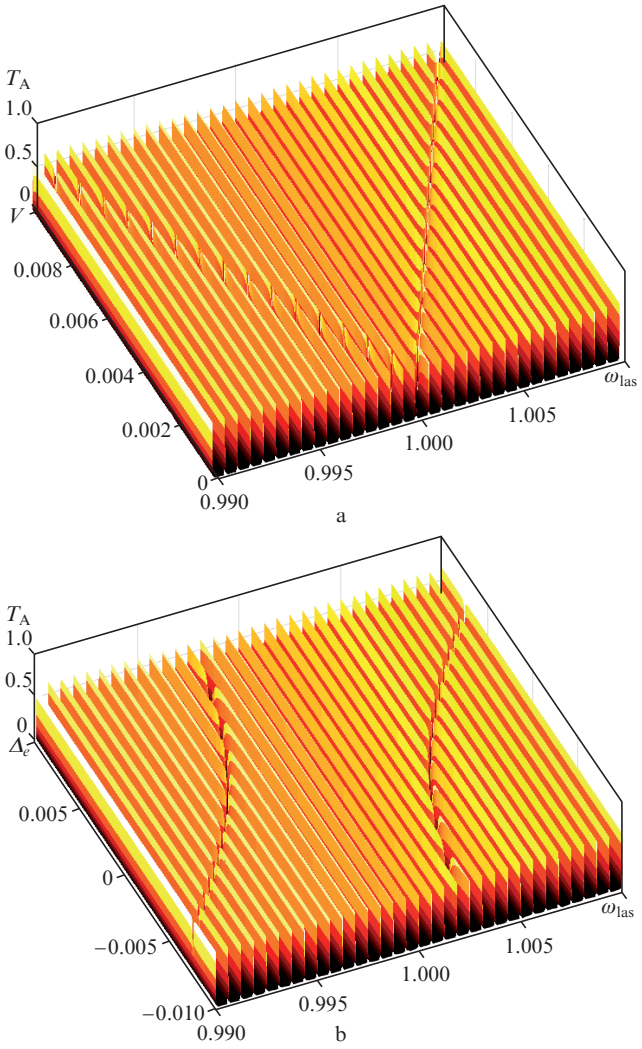

Figure 5. Photon transmittance as a function of laser frequency and DQD parameters – tunnelling energy (a) and the difference in excited state energy between the QDs A and B (b) – for a waveguide interacting with the electronic transition in the QD A: FSR $= 6\times10^{-4}$, $\Omega_{las} = 0.8\times10^{-5}$, $\Omega_A = 2\times10^{-5}$, $\kappa = 10^{-5}$, $\Delta_e = 0$, $\Delta_g = 10^{-3}$, and $V = 5\times10^{-3}$.

Another factor having a significant effect on the maximum contrast is the rate of photon dissipation from waveguide modes to a continuum. In a single-mode case, varying κ within one order of magnitude is accompanied by sharp changes in the function S_{max}. The reason for this is that, near resonance, the capacity of the structure is determined by the Ω_{las}^2/κ^2 ratio, and at a given pump rate the parameter κ determines the average number of transmitted photons. As shown earlier, the waveguide mode density (at constant Ω_A for all modes and some value of κ) influences the maximum contrast: the higher the mode density, the larger the difference between transmittances T_A and T_{wg}, which ensures S_{max} optimisation (Fig. 6). It can be seen that the simulation results on a steady-state response of a multimode waveguide with a QD in the Markov approximation indicate that mea-

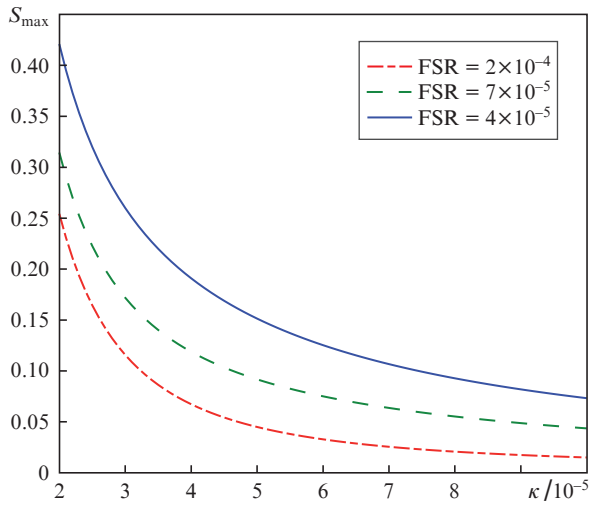

Figure 6. Maximum contrast as a function of photonic mode decay rate at three free spectral ranges, $\omega_{las} = 1 - V$, $\Omega_{las} = 10^{-5}$, $\Omega_A = 8 \times 10^{-5}$, $\Delta_e = 0$, $\Delta_g = 10^{-2}$, $V = 5 \times 10^{-3}$, and $\gamma = 2 \times 10^{-5}$.

surement contrast increases upon (a) a decrease in photon state decay rate, (b) an increase in mode–QD interaction energy, and (c) an increase in the density of waveguide mode states.

It should, however, be kept in mind that the mode density and mode field amplitudes (and, hence, interaction energies) are not separate parameters but depend on the waveguide length. At a constant waveguide cross section, an increase in waveguide length L is accompanied by an increase in the density of photon states and a decrease in mode field amplitude at a given point because of the field delocalisation along the waveguide. Besides, in the case of a discrete spectrum the Markov approximation $\Omega_{Ak} \approx \Omega_A$, usually applied in the theory of waveguides with a quasi-continuous photon mode distribution in the allowed band, can be invalid. In such a case, the set of Ω_{Ak} interaction energies should be calculated in a more exact model. Finally, the laser pump rate Ω_{las} controls the energy density inside the structure, having a strong effect on its transmittance owing to electromagnetic energy accumulation in the waveguide modes. This parameter is the most amenable to external control and can take values from zero to some maximum value, determined by operating characteristics of the laser. It should be kept in mind that, when Ω_{las} reaches a certain value, the conditions for the single-photon regime are no longer fulfilled. As will be seen in Section 4, this reduces measurement contrast and, as a consequence, impairs accuracy in measurements of the electronic state of QDs.

4. Calculation of 1D PC transmittance in the multiphoton single-mode regime

Assume that the spectrum of a 1D PC has resolution which allows one to separate one mode of frequency ω_c near the transition frequency ω_{-A} in the QD A. Varying the pump rate leads to two effects that have opposite impacts on S_{max}. On the one hand, according to Eqn (4) an increase in Ω_{las} leads to an increase in output signal, thereby contributing to an increase in S_{max}. On the other, at an average mode population ($\langle n \rangle \geqslant 1$) the conditions for photon blockade are weaker, which leads to a decrease in S_{max} and SNR – because multiphoton components emerge in the region of the splitting of the states of the vacuum Rabi doublet – and, hence, to an increase in the function T_A near the mode frequency $\omega_{las} = \omega_c$. Let the frequency detuning between the QD A and mode be denoted as $\delta_0 = \omega_{-A} - \omega_c$. Recall that, in the case of exact resonance ($\delta_0 = 0$), the optimal contrast corresponds to the frequency $\omega_{las} = \omega_c$, at which the function T_{wg} has a maximum and the function T_A has a minimum. As follows from the effect of pump energy on the $P(n)$ weights for the $n = 1$, 2, and 3 Fock components of the photon mode field (Fig. 7), the system is in the single-photon regime when pumping is less effective than scattering. With increasing laser energy, the Fock components with $n > 1$ emerge one after another and the average number of photons exceeds unity. In addition, note that the vacuum component $P(0)$ remains prevalent.

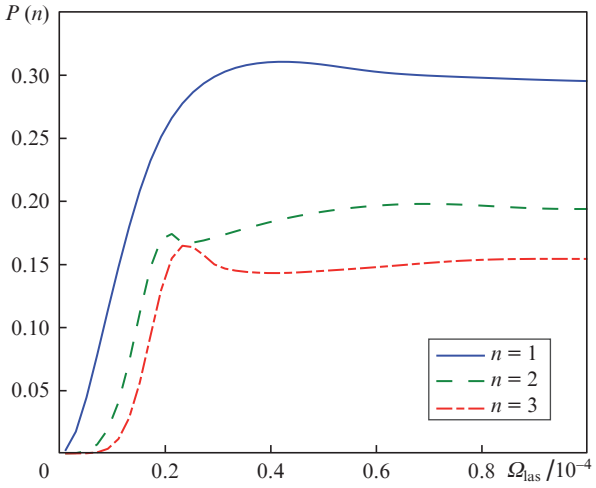

Figure 7. Populations of the first three Fock components of the waveguide mode field as functions of laser pump energy for exact resonance between the mode and QD A at $\Omega_A = 6 \times 10^{-5}$, $\delta_0 = 0$, $\kappa = 10^{-5}$, $\gamma_r = 10^{-6}$, and $\gamma_d = 10^{-5}$. The curves for $n \geqslant 4$ have a similar shape.

Figure 8 shows S_{max} as a function of pump energy at three frequency differences between the QD A and mode. In accordance with (4), the functions T_{wg}, T_A, and S vary quadratically with Ω_{las} in the subphoton pump regime ($\Omega_{las} \leqslant \kappa$). At $\Omega_{las} \approx \kappa$, the function S_{max} reaches a maximum, before decreasing as a consequence of the increase in T_A in the frequency range $\omega_c - \Omega_A \leqslant \omega_{las} \leqslant \omega_c + \Omega_A$ on account of the above-mentioned contribution of multiphoton states. The maximum value depends on detuning δ_0, which determines the efficiency of interaction between the QD A and mode at a constant energy Ω_A: the larger the detuning, the weaker is the effect of the QD A on the waveguide and the smaller is the difference between transmittances T_{wg} and T_A, which leads to a drop in contrast S and SNR. It is easy to understand that the optimal choice is exact resonance ($\delta_0 = 0$), which ensures the maximum difference between the functions T_{wg} and T_A at point $\omega_{las} = \omega_c$, corresponding to the maximum of the function S. Hereafter, we assume that conditions for exact frequency resonance in the system are fulfilled.

The effect of dissipative processes on the SNR on the whole reflects a general tendency for contrast to decrease, which is most clearly illustrated by dependences of the SNR on Ω_{las} at three rather close photonic mode decay rates

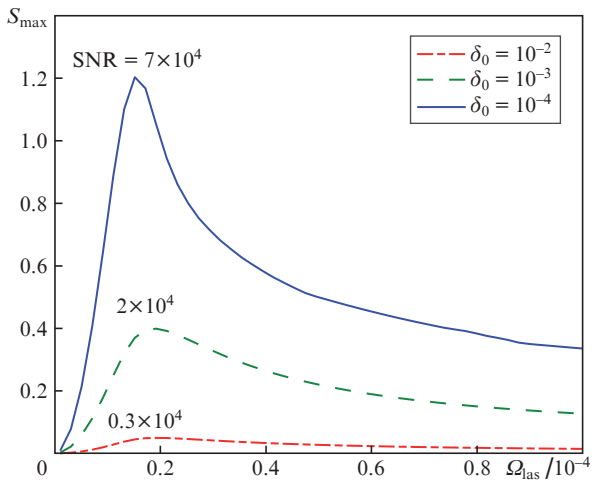

Figure 8. Maximum measurement contrast as a function of laser pump energy at three frequency differences between the QD A and mode, $\Omega_A = 6 \times 10^{-5}$, $\kappa = 10^{-5}$, $\gamma_r = 10^{-6}$, and $\gamma_d = 10^{-5}$. The numbers at the curves indicate optimal SNR values.

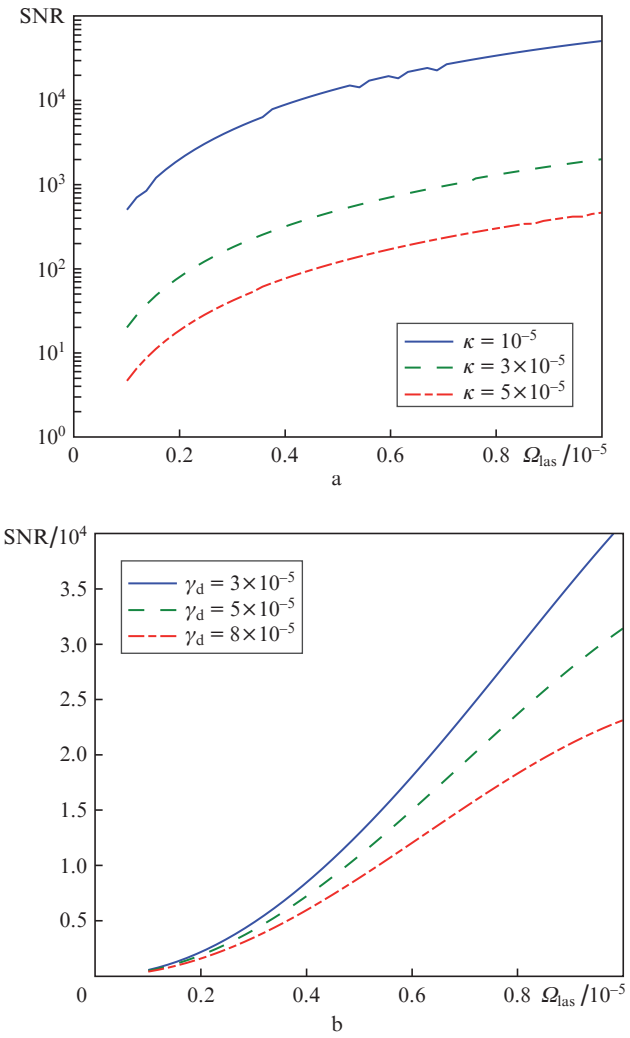

Figure 9. Signal-to-noise ratio as a function of laser pump energy at exact resonance between the mode and QD A for a varied photonic mode decay rate (a) and varied electronic transition dephasing rate in the QD A (b): $\Omega_A = 6 \times 10^{-5}$, $\delta_0 = 0$, $\gamma_r = 10^{-6}$, $\gamma_d = 10^{-5}$, and $\kappa = 10^{-5}$.

(Fig. 9a). Raising the pump energy from zero to 10^{-5} is accompanied by an increase in this function within two orders of magnitude, as in the case of a decrease in κ from 5×10^{-5} to 10^{-5}. Varying the transition dephasing rate in the QD, γ_d, from 3×10^{-5} to 8×10^{-5} at pump energies in the same range (Fig. 9b) causes less significant changes. The effect of the relaxation rate γ_r is still weaker. This is attributable to its dependence on the excited state population in the QD, which is much less than unity in this case. Note that low-dimensional structures have a quasi-discrete phonon spectrum dependent on parameters of the 1D PC, which allows one to control it, in particular by suppressing electron--phonon interaction and minimising the parameters γ_r and γ_d [42, 43].

Consider now the behaviour of measurement parameters as the energy of interaction between the QD A and waveguide mode, Ω_A, is varied. The monotonic increase in SNR between $\Omega_A = 0$ and $\Omega_A \approx \max(\kappa, \gamma_r, \gamma_d)$ is due to the field energy redistribution in the waveguide because of the presence of the QD. At $\Omega_A \approx 0$, the photon transmittance of the single-mode waveguide as a function of mode–laser frequency detuning has the form of a Lorentzian with a maximum at $\omega_{las} = \omega_c$. The effect of the QD A leads to a noticeable modification of the spectrum of the waveguide only at resonance, where the frequency detuning between the QD A and mode is smaller than Ω_A. As soon as the rate of coherent photon exchange between the waveguide and QD exceeds the rate of dissipative processes, the peak at the mode frequency splits into two polariton peaks (Jaynes–Cummings doublet) (Fig. 10). Here the rate γ_r is low compared to the other rates, so the spectrum has the form of a doublet, rather than a triplet, in contrast to what is described in Section 3.

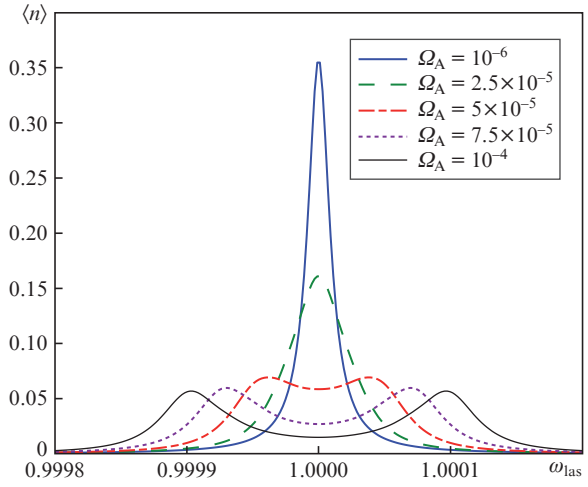

Figure 10. Average number of photons in the waveguide mode as a function of laser frequency at exact resonance between the mode and QD A, $\Omega_{las} = 6 \times 10^{-5}$, $\delta_0 = 0$, $\kappa = 10^{-5}$, $\gamma_r = 10^{-6}$, and $\gamma_d = 10^{-5}$. The variable parameter is the energy of interaction between the mode and the electronic transition of the QD A.

Their distinguishability can be quantified using the visibility function

$$C_{Rabi} = \left| [\langle n_{max} \rangle - \langle n_{max\,0} \rangle] / [\langle n_{max} \rangle + \langle n_{max\,0} \rangle] \right|, \qquad (7)$$

where $\langle n_{max\,0} \rangle$ is the average number of photons at frequency $\omega_{las} = \omega_c$ and $\langle n_{max} \rangle$ is the average number of photons at the

frequency of the local maximum. The $\langle n_{max} \rangle$ value coincides with $\langle n_{max\,0} \rangle$ before splitting and corresponds to one of the states of the doublet after splitting, whereas $\langle n_{max\,0} \rangle$ decreases monotonically to zero with increasing Ω_A. Accordingly, the function C_{Rabi} is zero before splitting and tends to unity with increasing Ω_A after splitting. In analysing the functions SNR and C_{Rabi} (Fig. 11), we note that their behaviour depends primarily on the parameters Ω_A, Ω_{las}, and κ. The interaction of the electronic transition in the QD with the waveguide mode through exchange of an energy quantum leads to splitting of the peak in question with increasing Ω_A. This is accompanied by a monotonic increase in C_{Rabi} and asymptotic behaviour of the SNR curve. Note that, even at low interaction energies, $\Omega_A \leqslant \kappa$, where the peak is still unsplit, its distortion due to the presence of the QD A ensures large SNRs. Another manifestation of the hybridisation of the electronic and photonic degrees of freedom is the dependence of the contrast peak width Γ_S on Ω_A (Fig. 11c). If there is no interaction between the mode and QD A, the full width at half maximum of the peak is $\Gamma_S \approx \kappa$, whereas after peak splitting at $\Omega_A \geqslant \kappa$ each polariton mode has a width $\Gamma_S \approx \kappa + \gamma_{r\,A}$, equal to the sum of the widths of the mode and QD A. In addition, the effect of the QD A on photon transport shows up as a population redistribution of the Fock components of the photon field (Fig. 11d). The spectrum of the mode of the waveguide with no QDs corresponds to the linear spectrum of a harmonic oscillator, whose frequency is independent of the number of photons.

The presence of a QD leads to fundamental changes in the spectrum of the electron–photon hybrid system because its eigenfrequencies become nonlinear (square root) functions of n. An increase in mode–QD interaction energy leads to stronger nonlinearity, increasing the frequency spacing between states of the system with different Fock components. The average number of photons in the mode is determined by the ratio of the laser (resonance) pump rate to the dissipation rate and decreases markedly compared to the waveguide with no QDs. As can be seen from Fig. 11, the single-photon regime sets in at $\Omega_{las} \leqslant \Omega_A$ and is maintained with high accuracy. In the case of exact mode–QD resonance, with increasing n the frequencies of the multiphoton components shift towards the mode frequency with no QDs ($\delta_0 = 0$), located halfway between the frequencies of the first (single-photon) Jaynes–Cummings doublet. In effect, the structure in question is a single-photon transistor in which the QD (qubit) serves not merely as a system being tested but as a functional nonlinear component of a measuring device.

Comparing the calculation results with experimental data obtained by differential reflectometry for an excitonic QD interacting with a microcavity mode [44, 45], we note that they are qualitatively similar. In particular, Englund et al. [44] clearly demonstrated a sharp drop in contrast (difference

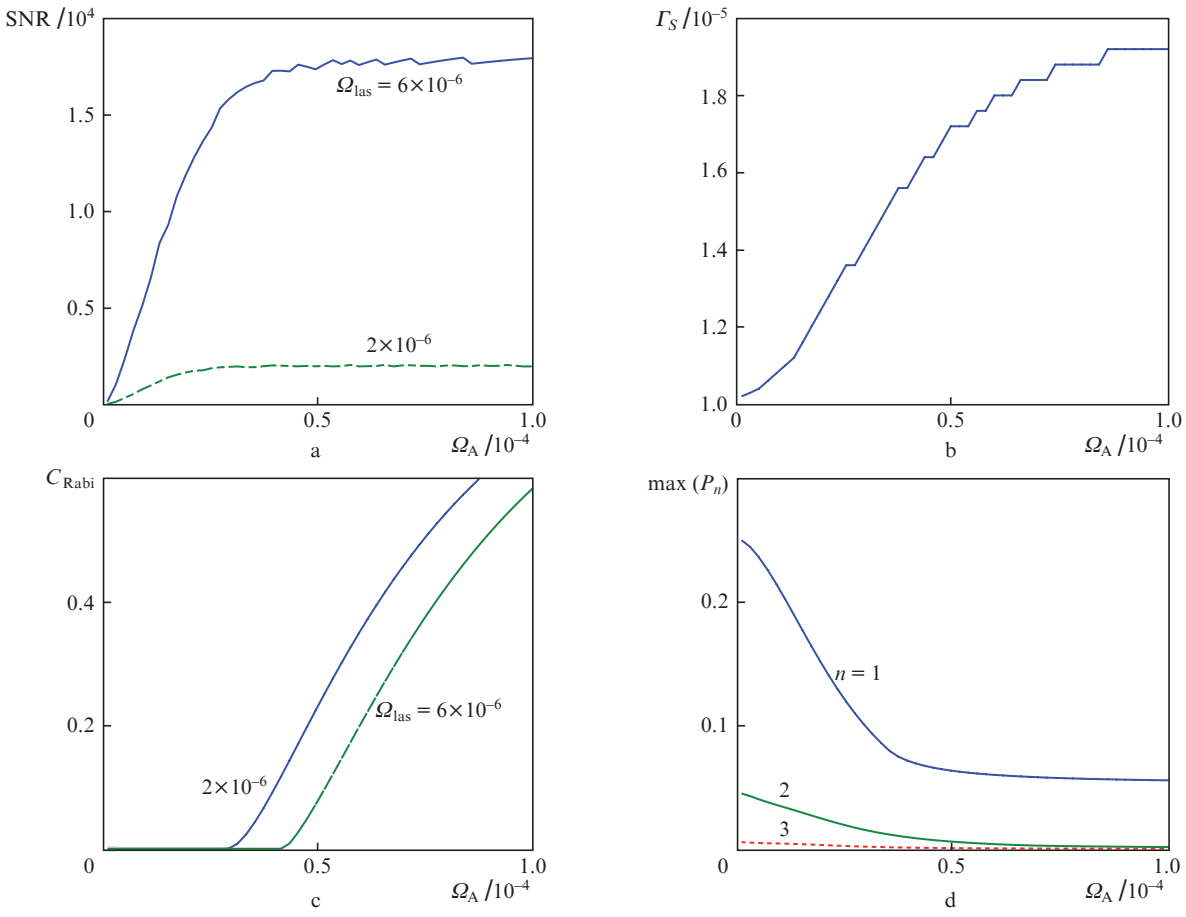

Figure 11. (a) Signal-to-noise ratio, (b) contrast peak width ($\delta_0 = 0$, $\kappa = 10^{-5}$, $\gamma_r = 10^{-6}$, and $\gamma_d = 10^{-5}$), (c) Jaynes–Cummings doublet visibility, and (d) maximum population of the first three Fock components of the mode ($\Omega_{las} = 6 \times 10^{-6}$) as functions of the energy of interaction between the mode and QD A in the case of exact resonance.

between the numbers of photons reflected from a cavity with and without a QD) upon a deviation from conditions of the subphoton pump regime ($\langle n \rangle \geqslant 0.5$) or an increase in mode–QD frequency detuning. The feasibility of using intermediate-Q modes is confirmed by measurements performed by Stumpf et al. [45]. The optimal SNR reached in their work is about 10^3 at a laser output power of 50 nW and wavelength of 780 nm [40]. A serious drawback to the reflectometric approach is the necessity to distinguish pump photons and reflected photons, having the same frequency, which requires that an additional polarisation block be incorporated into the chip scheme. In transmittance measurements, this can be achieved in a natural manner owing to their spatial separation due to the device geometry chosen.

5. Conclusions

The approach proposed in this study for detecting the presence or absence of an electron in a QD has an important practical application: measurement of a charge qubit. Traditionally, the internal state of a QD was probed using a single-electron transistor, whose operating temperature did not exceed a few kelvins [30]. It includes in the order of ten gate electrodes and supports only one qubit. An alternative technique for spectroscopic measurements on 1D QDs with the use of high-Q superconducting microwave cavities requires even lower temperatures (no higher than 0.1 K) [46]. On the other hand, to study the optical response of QDs in bulk crystals (without using quantum waveguide structures), strong laser fields should be used [25]. In such a case, a high source power is needed to compensate for losses due to photon scattering and absorption in the crystal. The minimum size of the irradiated region corresponds to the laser wavelength (of the order of 1–10 μm), whereas the spacing between neighbouring qubits is 500–800 nm. Both factors can lead to an undesirable effect of laser radiation on other qubits.

The scheme considered above allows one to obviate some technological difficulties because the photon source and DQD interact not directly but through a waveguide. In this case, the subphoton pump regime makes it possible to take advantage of quantum nonlinearity (photon blockade effect) for improving measurement reliability. At the same time, detuned from resonance with laser light, the other qubits are not influenced by the weak measuring field. Besides, a waveguide supporting a set of well-identifiable modes can serve several functions. In addition to being involved in the measurement process, it is suitable for performing individual coherent control over each qubit and organising nonlocal coupling between the qubits (including the generation of entangled states). For each operation, one mode or a few modes in different spectral regions are allocated. The critical temperature, above which electron–phonon effects actively influence the Q-factor of measurements on QDs with a transition energy from 50 to 100 meV is 30–50 K or even more.

Using the formalism of the Lindblad and Schrödinger equations, we calculated the response of a waveguide interacting with an asymmetric DQD (qubit) under steady-state laser pump conditions. Numerical simulation results on electron–photon dynamics demonstrate significant changes in the photon transmittance of the waveguide, due to resonance energy exchange with the QD. The pump energy, mode–QD interaction energy, and photon dissipation rate have the strongest effects on measurement contrast. A low waveguide mode density makes it possible to observe Rabi splitting and perform measurements in the photon blockade regime. It has been shown, however, that this is not a necessary criterion for high-accuracy detection because low-Q waveguides with a relatively low doublet structure resolution also have a rather high contrast.

A high mode density improves measurement effectiveness, but one then loses the possibility of selectively exciting individual modes, which is necessary for making coherent manipulations with qubits. An increase in pump field amplitude also has an ambiguous effect on contrast. On the one hand, it contributes to transmitted signal amplification. On the other, the excitation of multiphoton components in the splitting range considerably reduces contrast. It is this distinctive feature, characteristic of subphoton measurements, which sets the maximum contrast ($S_{\max} \sim 0.5–1$) and signal-to-noise ratio (SNR $\sim 10^4$ to 10^5) for optimising the other parameters of the 1D PC, laser, and DQD.

The feasibility of directly utilising the present results depends on experimental investigation of quantum-optical phenomena in single-electron QDs and DQDs with the use of quantum cascade lasers in the frequency range 10–50 THz. The configuration of the device in question is typical of transmission spectroscopy, which should facilitate its practical implementation. The theoretical results obtained in this study using a validated quantum-mechanical model suggest that there are rather wide ranges of parameters in which the described procedure for measuring the state of a charge qubit should ensure good accuracy. This gives grounds to expect successful experimental demonstration of the proposed approach.

Acknowledgements. The investigation was supported by Program No. 0066-2019-0005 of Ministry of Science and Higher Education of Russia for the Valiev Institute of Physics and Technology of RAS.*

References

1. Maddaloni P., Bellini M., De Natale P. *Laser-Based Measurements for Time and Frequency Domain Applications. A Handbook, Series in Optics and Optoelectronics* (Boka Raton: CRC Press, 2013).
2. Walmsley A. *Science*, **348**, 525 (2015).
3. Gazzano O., Solomon G.S. *J. Opt. Soc. Am. B*, **33**, C160 (2016).
4. Fang Y.-L., Baranger H.U. *Phys. Rev. A*, **91**, 053845 (2015).
5. Morichetti F., Ferrari C., Canciamilla A., Melloni A. *Laser Photonics Rev.*, **6**, 74 (2012).
6. Joyce B.A., Kelires P.C., Naumovets A.G., Vvedensky D.D. *Quantum Dots: Fundamentals, Applications, and Frontiers* (Dordrecht: NATO Science Series, 2003).
7. Kimble H. *Nature*, **453**, 1023 (2008).
8. Yang D., Duan B., Liu X., Wang A., Li X., Ji Y. *Micromachines*, **11**, 72 (2020).
9. Ohta R., Ota Y., Nomura M., Kumagai N., Ishida S., Iwamoto S., Arakawa Y. *Appl. Phys. Lett.*, **98**, 173104 (2011).
10. Javadi A., Söllner I., Arcari M., Hansen S.L., Midolo L., Mahmoodian S., Kirsanske G., Pregnolato T., Lee E.H., Song J.D., Stobbe S., Lodahl P. *Nat. Commun.*, **6**, 8655 (2015).
11. Bose R., Sridharan D., Kim H., Solomon G.S., Waks E. *Phys. Rev. Lett.*, **108**, 227402 (2012).
12. Fedichkin L., Yanchenko M., Valiev K.A. *Nanotechnology*, **11**, 387 (2000).
13. Tanamoto T. *Phys. Rev. A*, **61**, 022305 (2000).
14. Gorman J., Hasko D.G., Williams D.A. *Phys. Rev. Lett.*, **95**, 090502 (2005).

*The Acknowledgements section was translated by the author.

15. Sherwin M.S., Imamoglu A., Montroy T. *Phys. Rev. A*, **60**, 3508 (1999).
16. Openov L.A. *Phys. Rev. B*, **60**, 8798 (1999).
17. Oh J.H., Ahn D., Hwang S.W. *Phys. Rev. A*, **62**, 052306 (2000).
18. Li X.-Q., Arakawa Y. *Phys. Rev. A*, **63**, 012302 (2000).
19. Sanders G.D., Kim K.W., Holton W.C. *Phys. Rev. B*, **61**, 7526 (2000).
20. Tsukanov A.V., Openov L.A. *Semiconductors*, **38**, 91 (2004) [*Fiz. Tekh. Poluprovodn.*, **38**, 94 (2004)].
21. Paspalakis E., Kis Z., Voutsinas E., Terzis A.F. *Phys. Rev. B*, **69**, 155316 (2004).
22. Basharov A.M., Dubovis S.A. *Quantum Electron.*, **35**, 683 (2005) [*Kvantovaya Elektron.*, **35**, 683 (2005)].
23. Golovinskii P.A. *Semiconductors*, **48**, 760 (2014) [*Fiz. Tekh. Poluprovodn.*, **48**, 781 (2014)].
24. Tsukanov A.V. *Phys. Rev. A*, **85**, 012331 (2012).
25. Stinaff E.A., Scheibner M., Bracker A.S., Ponomarev I.V., Korenev V.L., Ware M.E., Doty M.F., Reinecke T.L., Gammon D. *Science*, **311**, 636 (2006).
26. de Vasconcellos S.M., Gordon S., Bichler M., Meier T., Zrenner A. *Nat. Photonics*, **4**, 545 (2010).
27. Zhukov A.E., Tsyrlin G.E., Reznik R.R., Samsonenko Yu.B., Khrebtov A.I., Kaliteevskii M.A., Ivanov K.A., Kryzhanovskaya N.V., Maksimov M.V., Alferov Zh.I. *Semiconductors*, **50**, 662 (2016) [*Fiz. Tekh. Poluprovodn.*, **50**, 674 (2016)].
28. Ikonnikov A.V., Marem'yanin K.V., Morozov S.V., Gavrilenko V.I., Pavlov A.Yu., Shchavruk N.V., Khabibulin R.A., Reznik R.R., Tsyrlin G.E., Zubov F.I., Zhukov A.E., Alferov Zh.I. *Tech. Phys. Lett.*, **43**, 662 (2017) [*Pis'ma Zh. Tekh. Fiz.*, **43**, 86 (2017)].
29. Schneider C., Huggenberger A., Sünner T., Heindel T., Strauss M., Göpfert S., Weinmann P., Reitzenstein S., Worschech L., Kamp M., Höfling S., Forchel A. *Nanotechnology*, **20**, 434012 (2009).
30. Kouwenhoven L.P., Austing D.G., Tarucha S. *Rep. Prog. Phys.*, **64**, 701 (2001).
31. Lu X.-Y., Wu J., Zheng L.-L., Zhan Z.-M. *Phys. Rev. A*, **83**, 042302 (2011).
32. Zhou X.R., Lee J.H., Salamo G.J., Royo M., Climente J.I., Doty M.F. *Phys. Rev. B*, **87**, 125309 (2013).
33. Beirne G.J., Hermannstadter C., Wang L., Rastelli A., Schmidt O.G., Michler P. *Phys. Rev. Lett*., **96**, 137401 (2006).
34. Zallo E., Trotta R., Krapek V., Huo Y.H., Atkinson P., Ding F., Sikola T., Rastelli A., Schmidt O.G. *Phys. Rev. B*, **89**, 241303(R) (2014).
35. Zinovyev V.A., Dvurechenskii A.V., Kuchinskaya P.A., Armbrister V.A. *Phys. Rev. Lett.*, **111**, 265501 (2013).
36. Blokhin S.A., Nadtochii A.M., Krasivichev A.A., Karachinskii L.Ya., Vasil'ev A.P., Nevedomskii V.N., Maksimov M.V., Tsyrlin G.E., Buravlev A.D., Maleev N.A., Zhukov A.E., Ledentsov N.N., Ustinov V.M. *Fiz. Tekh. Poluprovodn.*, **47**, 87 (2012).
37. Chatterjee A., Stevenson P., De Franceschi S., Morello A., de Leon N., Kuemmeth F. *E-print arXiv*, 2005.06564/cond-mat (2020).
38. Yariv A., Lindsey C., Sivan U. *J. Appl. Phys.*, **58**, 3669 (1985).
39. Khitrova G., Gibbs H.M., Kira M., Koch S.W., Scherer A. *Nat. Phys.*, **2**, 82 (2006).
40. Kim D., Majumdar A., Kim H., Petroff P., Vuckovic J. *Appl. Phys. Lett.*, **97**, 053111 (2010).
41. Notomi M., Kuramochi E., Tanabe T. *Nat. Photonics*, **2**, 741 (2008).
42. Tsukanov A.V., Kateev I.Yu. *Quantum Electron.*, **48**, 641 (2018) [*Kvantovaya Elektron.*, **48**, 641 (2018)].
43. Tsukanov A.V., Kateev I.Yu. *Quantum Electron.*, **48**, 1009 (2018) [*Kvantovaya Elektron.*, **48**, 1009 (2018)].
44. Englund D., Faraon A., Fushman I., Stoltz N., Petroff P., Vuckovic J. *Nature*, **450**, 857 (2007).
45. Stumpf W.C., Asano T., Kojima T., Fujita M., Tanaka Y., Noda S. *Phys. Rev. B*, **82**, 075119 (2010).
46. Frey T., Leek P.J., Beck M., Blais A., Ihn T., Ensslin K., Wallraf A. *Phys. Rev. Lett.*, **108**, 046807 (2012).